Journal of Nuclear Medicine, published on July 9, 2020 as doi:10.2967/jnumed.120.244400

^{18}F-SMBT-1: A Selective and Reversible Positron-Emission Tomography Tracer for Monoamine Oxidase-B Imaging

Running title: ^{18}F-SMBT-1, a novel MAO-B PET tracer

Ryuichi Harada,[1, 2] Yoshimi Hayakawa,[3] Michinori Ezura,[4] Pradith Lerdsirisuk,[3] Yiqing Du,[1] Yoichi Ishikawa,[3] Ren Iwata,[3] Miho Shidahara,[5] Aiko Ishiki,[2] Akio Kikuchi,[4] Hiroyuki Arai,[2] Yukitsuka Kudo,[2] Kazuhiko Yanai,[1,3] Shozo Furumoto,[3] Nobuyuki Okamura,[3,6]

1. Department of Pharmacology, Tohoku University School of Medicine, Sendai, Japan

2. Department of Geriatrics and Gerontology, Division of Brain Sciences, Institute of Development, Aging and Cancer, Tohoku University, Sendai, Japan

3. Cyclotron and Radioisotope Center, Tohoku University, Sendai, Japan

4. Department of Neurology, Tohoku University Graduate School of Medicine. 1-1 Seiryo-machi, Aoba-ku, Sendai, Japan

5. Department of Quantum Science and Energy Engineering, Tohoku University, Sendai, Japan

6. Division of Pharmacology, Faculty of Medicine, Tohoku Medical and Pharmaceutical University, Sendai, Japan

Corresponding author:

Ryuichi Harada

Department of Pharmacology, Tohoku University School of Medicine

2-1, Seiryo-machi, Aoba-ku, Sendai 9808575, Japan

Tel: +81-22-717-8058, Fax: +81-22-717-8060

E-mail: ryuichi.harada.c8@med.tohoku.ac.jp

Word count: 4,916 words

ABSTRACT

Reactive astrocytes play a key role in the pathogenesis of various neurodegenerative diseases. Monoamine oxidase-B (MAO-B) is one of the promising targets for the imaging of astrogliosis in the human brain. A novel selective and reversible MAO-B tracer, (*S*)-(2-methylpyrid-5-yl)-6-[(3-[^{18}F]fluoro-2-hydroxy)propoxy]quinoline, (^{18}F-SMBT-1), was successfully developed via lead optimization from first-generation tau positron-emission tomography (PET) tracer ^{18}F-THK-5351. **Methods:** SMBT-1 was radiolabeled with fluorine-18 using the corresponding precursor. The binding affinity of radiolabeled compounds to MAO-B was assessed using saturation and competitive binding assays. The binding selectivity of ^{18}F-SMBT-1 to MAO-B was evaluated by autoradiography of frozen human brain tissues. The pharmacokinetics (PK) and metabolism were assessed in normal mice after intravenous administration of ^{18}F-SMBT-1. A 14-day toxicity study following the intravenous administration of SMBT-1 was performed using rats and mice. **Results:** *In vitro* binding assays demonstrated a high binding affinity of SMBT-1 to MAO-B (K_D = 3.7 nM). In contrast, it showed low binding affinity to MAO-A and protein aggregates such as amyloid-β and tau fibrils. Autoradiographic analysis showed higher amounts of ^{18}F-SMBT-1 binding in the Alzheimer's disease (AD) brain sections than in the control brain sections. ^{18}F-SMBT-1 binding was completely displaced with reversible MAO-B inhibitor lazabemide, demonstrating the high selectivity of ^{18}F-SMBT-1 for MAO-B. Furthermore, ^{18}F-SMBT-1 showed a high uptake by brain, rapid washout, and no

radiolabeled metabolites in the brain of normal mice. SMBT-1 showed no significant binding to various receptors, ion channels, and transporters, and no toxic effects related to its administration were observed in mice and rats. **Conclusion:** ^{18}F-SMBT-1 is a promising and selective MAO-B PET tracer candidate, which would be useful for quantitative monitoring of astrogliosis in the human brain.

Key words: MAO-B; radiotracers; positron emission tomography; molecular imaging

INTRODUCTION

Reactive astrocytosis is the astrocyte response observed in various neurological disorders. It is characterized by distinct morphological alternations such as enlarged cell bodies and overexpression of glial fibrillary acidic protein, vimentin, and nestin (*1*). In neurodegenerative conditions, astrocytes turn reactive and secrete neurotoxic inflammatory cytokines (*1*). Reactive astrocytes also overexpress monoamine oxidase-B (MAO-B) in the outer membrane of the mitochondria. MAO-B, a major enzyme that metabolizes dopamine and histamine, is widely distributed in the human brain. Higher levels of MAO-B expression are physiologically observed in the basal forebrain, substantia nigra, basal ganglia, thalamus, and hippocampal uncus relative to the cerebellar cortex (*2*). MAO-B levels in whole brain regions also increase linearly in an age-dependent manner during normal aging processes (*2,3*). Elevated MAO-B levels in autopsy-confirmed Alzheimer's disease (AD) brains were observed in *in vitro* binding studies with selective MAO-B radioligands, such as ^{3}H-L-deprenyl and ^{3}H-lazabemide (*4-6*). In addition, MAO-B elevation was also observed in the postmortem brains of parkinsonian syndromes, progressive supranuclear palsy (PSP), and multiple system atrophy (MSA) (*7*). This indicates that MAO-B could be an attractive target for visualizing reactive astrocytes *in vivo* during neuroinflammatory processes. Much effort has been made to develop novel MAO-B positron-emission tomography (PET) tracers based on the chemical structure of selective MAO-B inhibitors (*8,9*). ^{11}C-L-deprenyl-D2 (DED) is the most commonly used PET tracer for imaging MAO-B in

the human brain (Figure 1). However, quantifying ^{11}C-DED binding is difficult due to the its irreversible binding. ^{11}C-SL25.1188, a reversible MAO-B PET tracer, was developed and used to human studies (*10*). The short half-life of carbon-11 (20 min) limits the clinical utility of these PET tracers. Therefore, several ^{18}F-labelled PET tracers have been developed for imaging MAO-B (*11-14*). ^{18}F-THK-5351 was originally designed to detect neurofibrillary tangles *in vivo*, and was found to bind MAO-B with high affinity (*15,16*). Clinical ^{18}F-THK-5351 PET studies demonstrated high tracer retention in sites susceptible to astrogliosis in various neurodegenerative conditions (*17-26*). The non-selective binding of THK-5351 to MAO-B and tau limits its clinical utility as a biomarker. Herein, lead optimization for generating a selective MAO-B binding tracer led to the development of (*S*)-(2-methylpyrid-5-yl)-6-[(3-[^{18}F]fluoro-2-hydroxy)propoxy]quinoline, (^{18}F-SMBT-1) (Figure 1), a novel radiolabeled tracer compound. Here, we report the preclinical binding, pharmacokinetics (PK), and metabolic properties of SMBT-1 and its derivatives.

MATERIALS AND METHODS

Synthesis of SMBT-1 and Its Derivatives

Methods for the synthesis and characterization of the tracer compounds are described in the supplementary data (Supplementary scheme 1-4).

Radiochemistry

[^{18}F]Fluoride produced by the ^{18}O(p, n)^{18}F reaction on enriched [^{18}O]H_2O with cyclotron, was separated from the irradiated target with a Sep-Pak Light Accell Plus QMA cartridge (Waters, MA), which was washed in advance with K_2CO_3 followed by water. The trapped [^{18}F]Fluoride was eluted with a solution of Kryptfix®222 (8 mg), K_2CO_3 (1.5 mg), acetonitrile (0.45 mL), and water (0.13 mL). The eluted solution was then used for subsequent radiofluorination. The solution was evaporated to dryness by azeotropic distillation with a He flow (300 mL/min) heating at 110°C with stirring. After drying, the tosylate precursor (*S*)-(2-methylpyrid-5-yl)-6-[[2-(tetrahydro-2H-pyran-2-yloxy)-3-tosyloxy]propoxy]quinoline, THK-5475; 2 mg) dissolved in dimethylsulfoxide (0.45 mL) was transferred and stirred at 110°C for 10 min. Next, hydrochloride aqueous solution (2M, 0.2 mL) was added to the reaction solution and stirred at 110°C for an additional 3 min for deprotection of the hydroxy group. The reaction was then quenched with potassium acetate aqueous solution (0.2 M, 4 mL), followed by solid phase extraction. The crude mixture was passed through the activated Sep-Pak tC18 Plus (Waters) and then washed with water. Radioactive products remaining the solid phase were eluted with 70% ethanol (0.7 mL) and diluted with water (0.12 mL), and then subjected to semi-preparative high-performance liquid chromatography (HPLC) (column: Inertsil® ODS-4 (GL Sciences, Inc., Tokyo, Japan); mobile phase: 20 mmol/L NaH_2PO_4/acetonitrile (67/33 for SMBT-1); flow rate: 5.0 mL/min). A detailed account of the optimized procedure is provided in

Supplementary Table 1. ^{18}F-SMBT-1 production was also achieved by one-pot microscale radiosynthesis (*27*). ^{18}F-THK-5351 was prepared as described previously (*15*). ^{18}F-Fluoroethyl harmine (FEH) was prepared from the corresponding precursor using the microscale radiosynthesis method, as previously described (*27*). ^{125}I-Ro 43-0463 was prepared as described previously (*11*). ^{18}F-SMBT-1, ^{18}F-THK-5351, ^{18}F-FEH, and ^{125}I-Ro 43-0463 were obtained in greater than 95% radiochemical purity after HPLC purification. The averages of decay-corrected radiochemical yields and molar activity at the end of ^{18}F-SMBT-1 synthesis were 39% and 414 GBq/μmol, respectively.

***In Vitro* Binding Studies**

^{3}H-THK-5351 (molar activity, 2.96 TBq/mmol; radiochemical purity, 98.9%) was custom-labeled by Sekisui Medical Inc. (Tokyo, Japan). ^{3}H-PiB (molar activity, 2.96 TBq/mmol; radiochemical purity, 99%) was obtained from American Radiolabeled Chemicals (Saint Louis, Mo). ^{3}H-MK-6240 (molar activity, 0.83 TBq/mmol; radiochemical purity, 99%) was obtained from ViTrax (Placentia, CA). Competitive binding assays were performed as previously described (*28*). ^{3}H-PiB (1 nM) and ^{3}H-MK-6240 (1.5 nM) were used as radioligands for amyloid and tau aggregates, respectively. An *in vitro* saturation binding assay was also performed using ^{18}F-labeled compounds as previously described (*29*). ^{18}F-FEH and recombinant MAO-A (M7316, Sigma-Aldrich) were used for an *in vitro* competitive binding assay against MAO-A. The off-rate

(k_{off}) was determined as previously described (*30*). All assays were performed at room temperature in quadruplicate, and the k_{off} was determined by GraphPad Prism 7.0. Correlation analysis between tracer binding and MAO-B activity was performed as previously described (*16*).

In Vitro Autoradiography

The Ethics Committee of the Tohoku University Graduate School of Medicine approved this study and all subjects provided a written informed consent. Postmortem brain sections from control subjects and AD patients were acquired from Tohoku University Brain Bank. *In vitro* autoradiography was performed as previously described (*16*). To account for MAO-B binding in the brain tissues, the reaction was incubated in the presence of the MAO-B inhibitor lazabemide (1 μM). After post-fixation in 4% paraformaldehyde for 30 min, adjacent frozen sections were immunostained with anti-MAO-B (1:400, Sigma-Aldrich, St Louis, MO), anti-tau (AT8, Innogenetics, Ghent, Belgium), and anti-β-amyloid (6F/3D, Dako, Glostrup, Denmark) antibodies.

Biodistribution Study in Normal Mice

All animal experimental protocols were approved by the Laboratory Animal Care Committee of Tohoku University. The biodistribution study was performed as previously described (*29*). The radiation dose and

mass dose for humans were estimated based on the biodistribution data from mice (*31*).

Metabolite Analysis

Male ICR mice (6 weeks old) were sacrificed by decapitation under anesthesia at 2, 10, 30 min after intravenous ^{18}F-SMBT-1 (19.4 MBq) administration, and the brain and cardiac blood were collected. Extraction and metabolite analysis were performed as previously described (*32*). To identify the major metabolite of ^{18}F-SMBT-1, *in vitro* enzyme assays were performed using human sulfotransferase 1E1 (SULT1E1) (Cypex Ltd, Dundee, UK) as described previously (*28*).

Receptor Binding Assays

Receptor binding screen assays were performed by Sekisui Medical Inc. Binding inhibition (%) was determined by competitive radioligand assays against 60 common neurotransmitter receptors, ion channels, and transporters, as previously described (*29*).

Animal Toxicity Studies

Acute toxicity studies were performed on Sprague-Dawley rats and ICR mice. A single intravenous dose of SMBT-1 was administered by LSI Medience Inc. (Tokyo, Japan), as previously described (*29*).

RESULTS

In Vitro Competitive Binding Studies

We performed an *in vitro* competitive binding assay using ^{3}H-THK-5351 to measure the binding affinity of various compounds against recombinant MAO-B (Supplementary Table 2). Arylquinoline (AQ) derivatives including THK-5105 showed high binding affinity to MAO-B. The binding affinity of THK-5105 to MAO-B was substantially reduced following substitution of the hydroxy group in the (3-fluoro-2-hydroxy)propoxyl group by hydrogen. The chirality of compounds was also associated with the binding affinity to MAO-B. For example, *R*-enantiomer (THK-5451) showed lower affinity to MAO-B than *S*-enantiomer (THK-5351). Previous analysis of the structure-activity relationship (SAR) of 2-AQ derivatives showed that the 2 amino groups on the pyridine ring were essential for binding to tau aggregates (unpublished data). We therefore investigated the substituent on the pyridine ring at the 2-position to ensure high selectivity of compounds for MAO-B over tau aggregates. Although the hydrogen substituent on the pyridine ring (SMBT-0) reduced the binding affinity to MAO-B, the methyl substituent (SMBT-1) maintained a high binding affinity to MAO-B at a level comparable to THK-5351 and several other MAO-B inhibitors, such as rasagiline, lazabemide, and safinamide. Our SAR study of SMBT-1 derivatives demonstrated that the 2-methylpyridine derivative was the most ideal for generating high binding affinity

to MAO-B (Supplementary table 2). The binding of SMBT-1 to recombinant MAO-A was further investigated by an *in vitro* competitive binding assay using the reversible MAO-A binder ^{18}F-FEH. In contrast with its high affinity to MAO-B, SMBT-1 showed low binding affinity to MAO-A (IC_{50} = 713 nM). Furthermore, SMBT-1 showed low binding affinity to amyloid-β and tau protein aggregates (IC_{50} > 1,000 nM) (Supplementary Table 3). Receptor binding screen assays demonstrated no remarkable interaction with various receptors, ion channels, and transporters (Supplementary Table 4).

In Vitro Binding Studies of ^{18}F-SMBT-1 to MAO-B

Next, we radiolabeled SMBT-1 with fluorine-18 and investigated the binding properties of ^{18}F-SMBT-1 to MAO-B in detail. Saturation binding assays demonstrated a high binding affinity of ^{18}F-SMBT-1 for recombinant MAO-B (K_D = 3.7 nM, B_{max} = 110.4 pmol/mg protein) (Figure 2). As shown in Supplementary Figure 1, ^{18}F-SMBT-1 also showed high binding affinity for MAO-B-rich AD brain homogenates (K_D = 3.5 nM) and mouse brain homogenates (K_D = 4.3 nM). However, the B_{max} in AD brain homogenates (606 pmol/g tissue) was approximately 3 times higher than that in mouse brain homogenates (153 pmol/g tissue). The specific binding of ^{18}F-SMBT-1 to human AD brain homogenates and recombinant MAO-B was reversible with similar kinetics (Fig. 3B). The k_{off} values were determined to be 0.0087 min^{-1} and 0.0072 min^{-1} for human AD brain homogenate and recombinant MAO-B, respectively.

A strong correlation was observed between regional *in vitro* ^{18}F-SMBT-1 binding and MAO-B activity in a patient with AD (Spearman $r = 0.923$, $P < 0.0001$; Figure 3). We also observed a significant correlation with sarkosyl insoluble tau (Spearman $r = 0.678$, $P = 0.0049$); however, this association was weaker than that observed with MAO-B activity. In contrast, no significant correlation was observed with insoluble total Aβ (Spearman $r = -0.391$, $P = 0.135$).

In Vitro Autoradiography of Postmortem Human Brain Sections

In vitro autoradiography of ^{18}F-SMBT-1 was conducted to further evaluate the binding selectivity of SMBT-1 in human brain sections. Specific binding of ^{18}F-SMBT-1 was greater in human AD brain sections than in control brain sections, which was consistent with the results of MAO-B immunohistochemistry (Figure 4). These specific binding of ^{18}F-SMBT-1 was completely displaced in the presence of selective MAO-B inhibitor lazabemide, although ^{18}F-THK-5351 binding remained detectable in human AD brain sections after lazabemide treatment. The distribution of ^{18}F-SMBT-1 was also consistent with that of the reversible MAO-B tracer, ^{125}I-Ro 43-0463 (Supplementary Figure 2). Considerable amounts of ^{3}H-PiB and ^{3}H-MK-6240 binding were detected in these sections. These results indicate that ^{18}F-SMBT-1 binds to MAO-B with high selectivity.

Biodistribution of ^{18}F-SMBT-1 in Mice

^{18}F-SMBT-1 showed excellent blood-brain barrier permeability in mice. The peak uptake of ^{18}F-SMBT-1 (7.85 ± 0.76 %ID/g at 2 min p.i.) by the brain was greater than that of ^{18}F-THK-5351. Furthermore, ^{18}F-SMBT-1 showed rapid washout from normal brain tissue and no significant defluorination in mice (Table 1). ^{18}F-SMBT-1 radiation exposure was estimated from the biodistribution data from mice (Supplementary Table 5). The resultant whole-body effective dose equivalents were 12.2 μSv/MBq (male) and 21.3 μSv/MBq (female), which were comparable to those of ^{18}F-THK-5351 (*15*).

***In Vivo* Metabolism in Mice**

The extraction efficiencies from blood and brain were 89% and 87%, respectively. Figure 5 shows the time-activity kinetics of radiolabeled metabolites and ^{18}F-SMBT-1 in the brain (A) and plasma (B). ^{18}F-SMBT-1 was dominantly metabolized to one polar metabolite. In plasma, 92%, 65%, and 19% of the parent compound remained at 2, 10, and 30 min post-injection, respectively. On the other hand, most of the radioactivity in the brain was derived from the parent compound during the 30-minute period after intravenous administration. As previously observed in ^{18}F-THK-5351 (*28*), the major metabolite M2 exhibited the same R_f value as enzymatically produced *O*-sulfated SMBT-1.

Animal Toxicity Studies

A single intravenous administration of SMBT-1 at 1 mg/kg, equivalent to 100,000-fold the intended clinical dose for humans, caused no systemic toxicity in rats or mice.

DISCUSSION

^{18}F-SMBT-1 is a single *S*-enantiomer and 2-methylpyridine derivative of ^{18}F-THK-5351. ^{18}F-THK-5351 was originally designed to detect tau aggregates in the form of paired helical filaments. However, recent studies showed high amounts of ^{18}F-THK-5351 binding to MAO-B. Recent clinical studies have demonstrated the unique pattern of ^{18}F-THK-5351 binding in various neurodegenerative diseases other than AD. However, the lack of binding selectivity of this tracer makes it difficult to interpret PET images. Therefore, we conducted lead optimization of THK-5351 derivatives to determine a selective MAO-B binding profile and a favorable PK profile. Previous SAR analysis of 2-AQ derivatives showed that the 2-amino group on the pyridine ring of 2-AQ derivatives was essential for binding to tau aggregates. In the present study, SAR analysis of MAO-B revealed that the hydroxy group in the (3-fluoro-2-hydroxy)propoxyl group of 2-AQ plays an important role in achieving high binding affinity for MAO-B; (3-fluoro-2-hydroxy)propoxyl group has a chiral center. Previous studies demonstrated that the *S*-enantiomers of THK compounds showed better PK than the *R*-enantiomers (*30,32*). In addition, the present

study demonstrated the higher affinity of the *S*-enantiomer for MAO-B compared to the *R*-enantiomer. Therefore, we selected the *S*-enantiomer as the novel MAO-B tracer candidate. We further explored the functional group at position 2 on the pyridine ring to reduce the binding affinity for tau aggregates. Among several derivatives, SMBT-1 showed the highest affinity for MAO-B and an excellent binding selectivity for MAO-B over MAO-A, amyloid, and tau aggregates. These findings were supported by *in vitro* autoradiography of ^{18}F-SMBT-1 using human brain tissues.

The binding of the radiotracer can be predicted by the ratio of the number of binding sites (B_{max}) to the binding affinity (K_D) for the target. ^{18}F-SMBT-1 showed low K_D and high B_{max} values (K_D = 3.7 nM, B_{max} = 110.4 pmol/mg protein) against recombinant MAO-B and human brain homogenates (K_D = 3.5 nM, B_{max} = 606 pmol/g tissue). The binding potential (B_{max}/K_D) was greater than currently available tau PET tracers, suggesting the ability of ^{18}F-SMBT-1 to detect MAO-B *in vivo*. MAO-B levels in the human brain cortex were 2.5–4.7-fold higher than those in rodents (*33*). This was consistent with the B_{max} value determined via *in vitro* ^{18}F-SMBT-1 binding assays. Since MAO-B is predominantly expressed in humans, but not in rodents, the differences in MAO expression between these species should be considered when using ^{18}F-SMBT-1 in preclinical studies.

Classical MAO-B PET tracers based on MAO-B inhibitors such as ^{11}C-pargyline, ^{11}C-L-deprenyl, and ^{18}F-rasagiline show irreversible binding to MAO-B. This is due to the formation of a covalent adduct with

flavin adenine dinucleotide (FAD), which is a redox-active coenzyme associated with MAO-B (*34-36*). The irreversibility of tracer binding led to an underestimation of MAO-B in the high concentration regions, as the rate of tracer binding may exceed the rate of tracer delivery (*37*). Deuterium-substituted radiotracers such as ^{11}C-DED, ^{18}F-fluorodeprenyl-D2, and ^{18}F-rasagiline-D2 reduce the trapping rate of the tracers and partly overcome these limitations; however they still possessed irreversible binding properties for MAO-B. Reversible radiotracers would be preferable for sensitive and quantitative MAO-B detection *in vivo*. Carbon-11 limits the use of the radiotracer to centers with an on-site cyclotron and ^{11}C radiochemistry expertise. ^{18}F-labeling of SMBT-1 permits centralized production and regional distribution of the radiotracer. The *in vitro* binding kinetics of ^{18}F-SMBT-1 demonstrated its reversible binding to MAO-B in human brains. The advantages of ^{18}F-SMBT-1 in terms of its reversibility would allow us to perform repeated PET scans in the same subject. This will help in longitudinal quantification of astrogliosis and measurement of MAO-B occupancy via therapeutics.

^{18}F-SMBT-1 showed excellent PK profiles, such as high uptake by brain after intravenous administration, and rapid washout from normal brain tissues without significant defluorination in mice. These characteristics were comparable to those of ^{18}F-THK-5351. One of the drawbacks of ^{11}C-DED is the existence of radiolabeled metabolites, such as (*R*(-)-methamphetamine and *R*(-)-amphetamine) that can penetrate the blood-brain barrier (BBB) and bind to monoamine transporters. Conversely, the reversible

MAO-B PET tracer ^{11}C-SL.25.1188 showed no BBB-permeable radiolabeled metabolites. However, this tracer showed slow PK due to slow metabolism (*10,38*). ^{18}F-SMBT-1 was completely metabolized in mice without leaving harmful radiolabeled metabolite remnants. The dominant radiolabeled metabolite (M2) in mouse plasma was *O*-sulfated SMBT-1, which was not detectable in the mouse brain. A previous study demonstrated that *O*-sulfated THK-5351 did not penetrate the BBB in mice and showed little binding to human brain homogenates (*28*). This evidence suggests that the *in vivo* metabolic profile of SMBT-1 could be suitable for MAO-B imaging in the brain.

CONCLUSION

^{18}F-SMBT-1 is a promising candidate as a selective and reversible imaging tracer for MAO-B. Ongoing clinical study will allow us to classify the clinical utility of this tracer *in vivo*.

STATEMENT OF DISCLOSURE

This study was supported by Cino Ltd, Grant-in-Aid for Young Scientists (18K15538), Grant-in-Aid for Scientific Research (B) (18H02771), Grant-in-Aid for Scientific Research on Innovative Areas (Brain Protein Aging and Dementia Control) (26117003), Grant-in-Aid for Fostering Joint International Research (B) (19KK0212) from MEXT, the Strategic Research Program for Brain Science (19dm0107157h0001)

from the Japan Agency for Medical Research and Development, and Grant-in-Aid for Joint Research by Young Researchers from Tohoku University Graduate School of Medicine and Shimadzu Science Foundation. Drs Kudo and Okamura own stock in Clino Ltd. Drs Harada, Furumoto, Kudo, and Okamura have a patent pending for the technology described in this manuscript. No other potential conflicts of interest relevant to this article exist.

ACKNOWLEDGMENTS

We are grateful to the staff at Cyclotron and Radioisotope Center of Tohoku University for the HM-12 cyclotron operation. We acknowledge the support of the Biomedical Research Core of Tohoku University Graduate School of Medicine.

Key Points:

Question: What are the preclinical properties of a newly generated MAO-B tracer, ^{18}F-SMBT-1, compared to ^{18}F-THK-5351?

Pertinent Findings: We developed a novel MAO-B PET tracer, ^{18}F-SMBT-1. ^{18}F-SMBT-1 possess high affinity and high selectivity for MAO-B in a reversible binding fashion with preferable pharmacokinetic and metabolic profiles.

Implications for Patient Care: Our results indicate potential use of ^{18}F-SMBT-1 for detection of MAO-B expressing astrocytosis in humans.

REFERENCES

1. Carter SF, Herholz K, Rosa-Neto P, Pellerin L, Nordberg A, Zimmer ER. Astrocyte biomarkers in Alzheimer's disease. *Trends Mol Med.* 2019;25:77-95.

2. Tong J, Meyer JH, Furukawa Y, et al. Distribution of monoamine oxidase proteins in human brain: implications for brain imaging studies. *J Cereb Blood Flow Metab.* 2013;33:863-871.

3. Fowler JS, Volkow ND, Wang GJ, et al. Age-related increases in brain monoamine oxidase B in living healthy human subjects. *Neurobiol Aging.* 1997;18:431-435.

4. Jossan SS, Gillberg PG, d'Argy R, et al. Quantitative localization of human brain monoamine oxidase B by large section autoradiography using L-[^{3}H]deprenyl. *Brain Res.* 1991;547:69-76.

5. Saura J, Luque JM, Cesura AM, et al. Increased monoamine oxidase B activity in plaque-associated astrocytes of Alzheimer brains revealed by quantitative enzyme radioautography. *Neuroscience.* 1994;62:15-30.

6. Gulyas B, Pavlova E, Kasa P, et al. Activated MAO-B in the brain of Alzheimer patients, demonstrated by [^{11}C]-L-deprenyl using whole hemisphere autoradiography. *Neurochem Int.* 2011;58:60-68.

7. Tong J, Rathitharan G, Meyer JH, et al. Brain monoamine oxidase B and A in human parkinsonian dopamine deficiency disorders. *Brain.* 2017;140:2460-2474.

8. Fowler JS, Logan J, Shumay E, Alia-Klein N, Wang GJ, Volkow ND. Monoamine oxidase: radiotracer chemistry and human studies. *J Labelled Comp Radiopharm.* 2015;58:51-64.

9. Narayanaswami V, Drake LR, Brooks AF, et al. Classics in neuroimaging: development of PET tracers for imaging monoamine oxidases. *ACS Chem Neurosci.* 2019;10:1867-1871.

10. Rusjan PM, Wilson AA, Miler L, et al. Kinetic modeling of the monoamine oxidase B radioligand [^{11}C]SL25.1188 in human brain with high-resolution positron emission tomography. *J Cereb Blood Flow Metab.* 2014;34:883-889.

11. Blauenstein P, Remy N, Buck A, et al. In vivo properties of N-(2-aminoethyl)-5-halogeno-2-pyridinecarboxamide 18F- and 123I-labelled reversible inhibitors of monoamine oxidase B. *Nucl Med Biol* 1998;25:47-52.

12. Nag S, Lehmann L, Kettschau G, et al. Development of a novel fluorine-18 labeled deuterated fluororasagiline ([F-18]fluororasagiline-D-2) radioligand for PET studies of monoamino oxidase B. *Bioorgan Med Chem* 2013;21:6634-6641

13. Nag S, Fazio P, Lehmann L, et al. In vivo and in vitro characterization of a novel mao-b inhibitor radioligand, 18f-labeled deuterated fluorodeprenyl. *J Nucl Med.* 2016;57:315-320.

14. Dahl K, Bernard-Gauthier V, Nag S, et al. Synthesis and preclinical evaluation of [^{18}F]FSL25.1188, a reversible PET radioligand for monoamine oxidase-B. *Bioorg Med Chem Lett.* 2019;29:1624-1627.

15. Harada R, Okamura N, Furumoto S, et al. ^{18}F-THK5351: A novel pet radiotracer for imaging neurofibrillary pathology in Alzheimer disease. *J Nucl Med.* 2016;57:208-214.

16. Harada R, Ishiki A, Kai H, et al. Correlations of ^{18}F-THK5351 pet with postmortem burden of tau and astrogliosis in Alzheimer disease. *J Nucl Med.* 2018;59:671-674.

17. Ishiki A, Harada R, Okamura N, et al. Tau imaging with [^{18} F]THK-5351 in progressive supranuclear palsy. *Eur J Neurol.* 2017;24:130-136.

18. Kikuchi A, Okamura N, Hasegawa T, et al. In vivo visualization of tau deposits in corticobasal syndrome by ^{18}F-THK5351 PET. *Neurology.* 2016;87:2309-2316.

19. Kobayashi R, Hayashi H, Kawakatsu S, et al. [^{18}F]THK-5351 PET imaging in early-stage semantic variant primary progressive aphasia: a report of two cases and a literature review. *BMC Neurol.* 2018;18:109.

20. Lee H, Seo S, Lee SY, et al. [^{18}F]-THK5351 PET imaging in patients with semantic variant primary progressive aphasia. *Alzheimer Dis Assoc Disord.* 2018;32:62-69.

21. Ishibashi K, Miura Y, Hirata K, Toyohara J, Ishii K. ^{18}F-THK5351 PET can identify astrogliosis in multiple sclerosis plaques. *Clin Nucl Med.* 2020;45:e98-e100.

22. Schonecker S, Brendel M, Palleis C, et al. PET imaging of astrogliosis and tau facilitates diagnosis of parkinsonian syndromes. *Front Aging Neurosci.* 2019;11:249.

23. Tago T, Toyohara J, Sengoku R, Murayama S, Ishii K. Monoamine oxidase b binding of ^{18}F-thk5351 to visualize glioblastoma and associated gliosis: an autopsy-confirmed case. *Clin Nucl Med.* 2019;44:507-509.

24. Ishibashi K, Kameyama M, Tago T, Toyohara J, Ishii K. Potential use of ^{18}F-THK5351 PET to identify Wallerian degeneration of the pyramidal tract caused by cerebral infarction. *Clin Nucl Med.* 2017;42:e523-e524.

25. Kim HJ, Cho H, Park S, et al. THK5351 and flortaucipir PET with pathological correlation in a Creutzfeldt-Jakob disease patient: a case report. *BMC Neurol.* 2019;19:211.

26. Huang KL, Hsu JL, Lin KJ, et al. Visualization of ischemic stroke-related changes on ^{18}F-THK-5351 positron emission tomography. *EJNMMI Res.* 2018;8:62.

27. Iwata R, Pascali C, Terasaki K, Ishikawa Y, Furumoto S, Yanai K. Practical microscale one-pot radiosynthesis of ^{18}F-labeled probes. *J Labelled Comp Radiopharm.* 2018;61:540-549.

28. Harada R, Furumoto S, Tago T, et al. Characterization of the radiolabeled metabolite of tau PET tracer ^{18}F-THK5351. *Eur J Nucl Med Mol Imaging.* 2016;43:2211-2218.

29. Okamura N, Furumoto S, Harada R, et al. Novel ^{18}F-labeled arylquinoline derivatives for noninvasive imaging of tau pathology in Alzheimer disease. *J Nucl Med.* 2013;54:1420-1427.

30. Tago T, Furumoto S, Okamura N, et al. Preclinical evaluation of [^{18}F]THK-5105 enantiomers: effects of chirality on its effectiveness as a tau imaging radiotracer. *Mol Imaging Biol.* 2016;18:258-266.

31. Shidahara M, Tashiro M, Okamura N, et al. Evaluation of the biodistribution and radiation dosimetry of the 18F-labelled amyloid imaging probe [18F]FACT. *EJNMMI Research.* 2013;3:32.

32. Tago T, Furumoto S, Okamura N, et al. Structure-activity relationship of 2-arylquinolines as PET imaging tracers for tau pathology in Alzheimer disease. *J Nucl Med.* 2016;57:608-614.

33. Saura J, Kettler R, Da Prada M, Richards JG. Quantitative enzyme radioautography with ^{3}H-Ro 41-1049 and ^{3}H-Ro 19-6327 in vitro: localization and abundance of MAO-A and MAO-B in rat CNS, peripheral organs, and human brain. *J Neurosci.* 1992;12:1977-1999.

34. Ishiwata K, Ido T, Yanai K, et al. Biodistribution of a positron-emitting suicide inactivator of monoamine oxidase, carbon-11 pargyline, in mice and a rabbit. *J Nucl Med.* 1985;26:630-636.

35. Fowler JS, MacGregor RR, Wolf AP, et al. Mapping human brain monoamine oxidase A and B with ^{11}C-labeled suicide inactivators and PET. *Science.* 1987;235:481-485.

36. Nag S, Lehmann L, Kettschau G, et al. Synthesis and evaluation of [^{18}F]fluororasagiline, a novel positron emission tomography (PET) radioligand for monoamine oxidase B (MAO-B). *Bioorg Med Chem.* 2012;20:3065-3071.

37. Fowler JS, Wang GJ, Logan J, et al. Selective reduction of radiotracer trapping by deuterium substitution: comparison of carbon-11-L-deprenyl and carbon-11-deprenyl-D2 for MAO B mapping. *J Nucl Med.* 1995;36:1255-1262.

38. Saba W, Valette H, Peyronneau MA, et al. [^{11}C]SL25.1188, a new reversible radioligand to study the monoamine oxidase type B with PET: preclinical characterisation in nonhuman primate. *Synapse.* 2010;64:61-69.

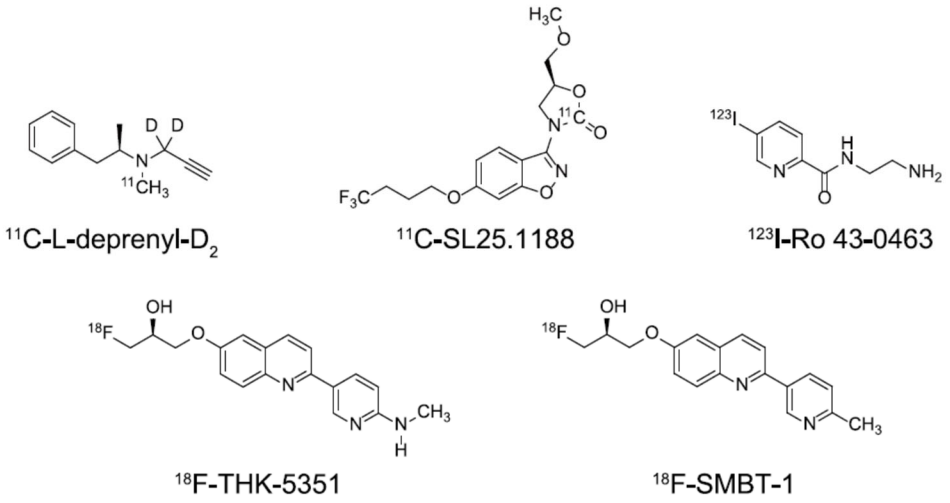

Figure 1. Chemical structures of monoamine oxidase-B (MAO-B) tracers tested in humans, ^{18}F-THK-5351 and ^{18}F-SMBT-1.

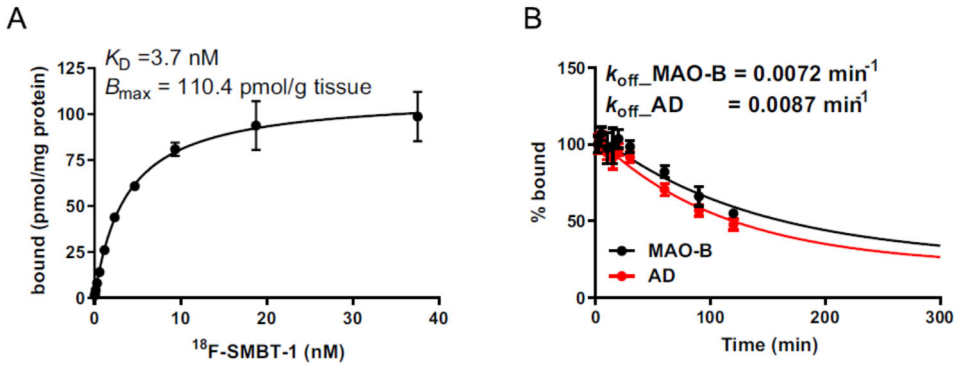

Figure 2. ***In vitro*** **saturation binding of ^{18}F-SMBT-1 against recombinant monoamine oxidase-B (MAO-B) (A).** ***In vitro*** **binding kinetics of ^{18}F-SMBT-1 against recombinant MAO-B and an Alzheimer's disease brain homogenate (B).**

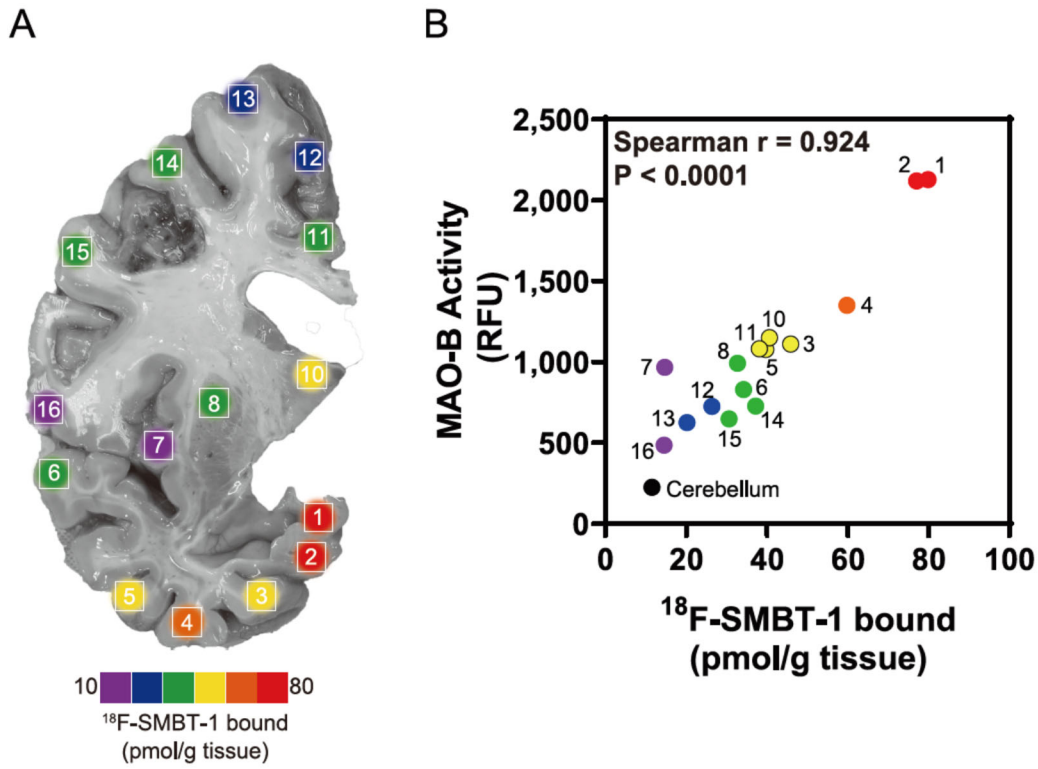

Figure 3. ^{18}F-SMBT-1 binding density map in 16 regions of coronal brain section of autopsy tissue from right hemisphere from a patient with Alzheimer's disease (81-year old male) (A). Correlation of regional *in vitro* ^{18}F-SMBT-1 binding and MAO-B activity (B).

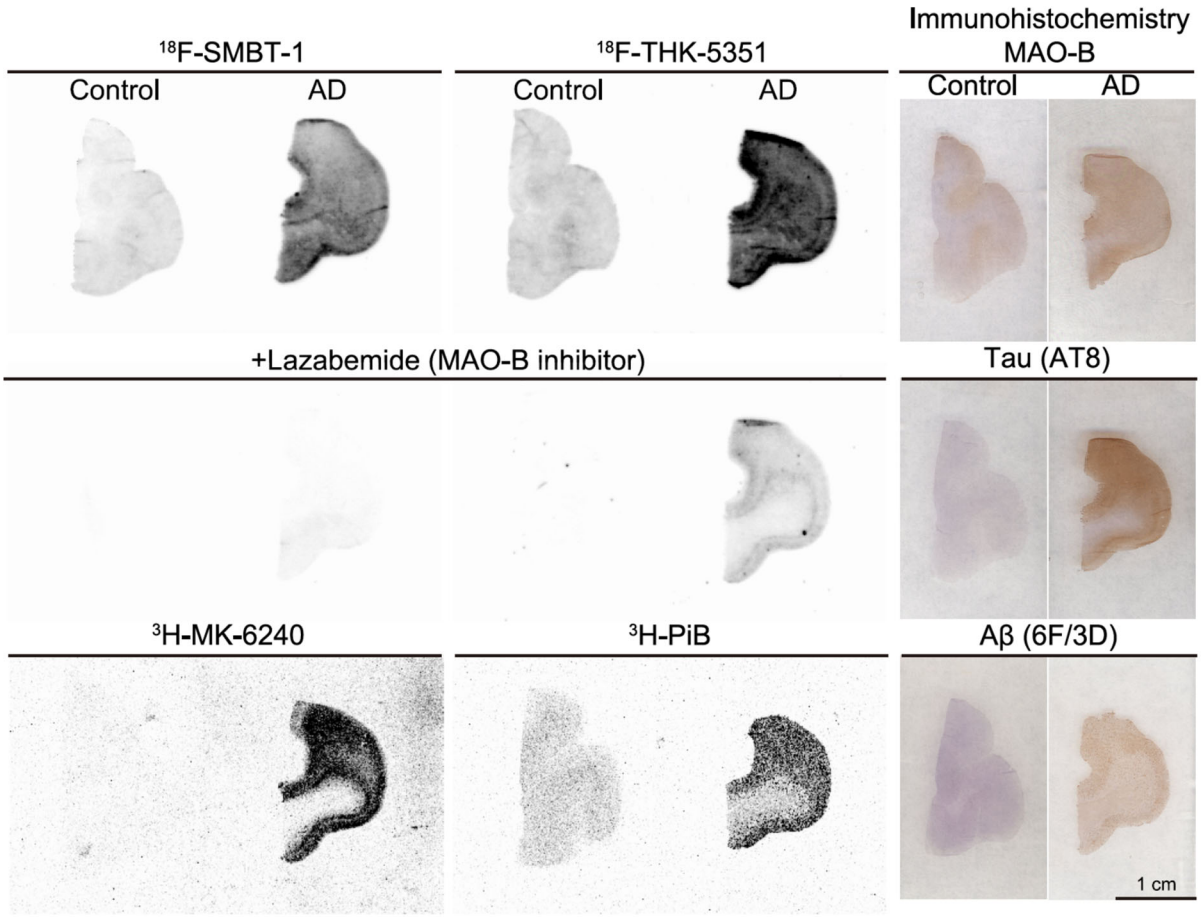

Figure 4. Comparative *in vitro* autoradiography of ^{18}F-SMBT-1, ^{18}F-THK-5351, ^{3}H-MK-6240, and ^{3}H-PiB in the frontal cortex of a control subject (55-year male) and a patient with Alzheimer's disease (68-year female). Adjusted sections were stained by anti- monoamine oxidase-B (MAO-B), anti-pTau (AT8), and anti-amyloid-β (6F/3D) antibodies.

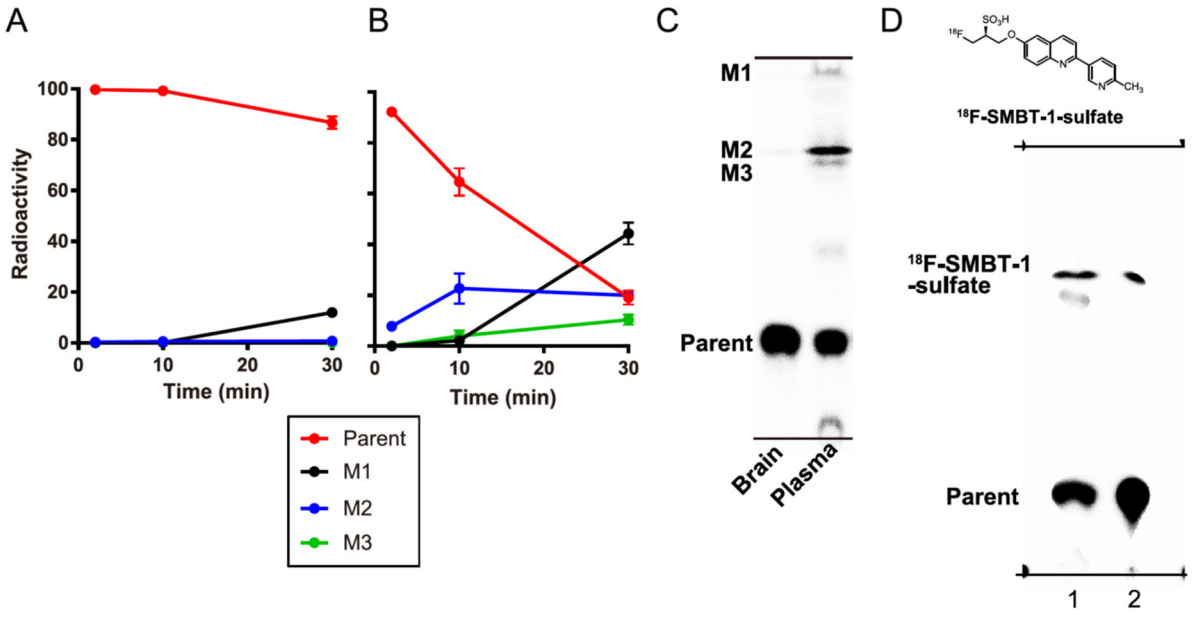

Figure 5. Time activity curves of parent and radiolabeled metabolites in brain (A) and plasma (B). Reverse phase thin-layer chromatography (RP-TLC) chromatograms (C). Chemical structure of *O*-sulfated ^{18}F-SMBT-1 by SULTE1E1 and RP-TLC chromatograms (D). Lane 1: Mouse plasma at 10 min post-injection of ^{18}F-SMBT-1, Lane 2: ^{18}F-SMBT-1 with SULTE1E1.

Table 1 Biodistribution after an intravenous injection of ^{18}F-SMBT-1 (%dose/g, avg of four mice (± SD)) in Institute of Cancer Research (ICR) mice

Organ	2 min	10 min	30 min	60 min	120 min
Blood	3.20 ± 0.45	1.28 ± 0.12	0.52 ± 0.10	0.28 ± 0.03	0.17 ± 0.04
Brain	7.85 ± 0.76	2.11 ± 0.35	0.32 ± 0.05	0.20 ± 0.02	0.14 ± 0.02
Liver	7.97 ± 1.72	13.7 ± 2.81	3.16 ± 1.10	1.35 ± 0.06	1.67 ± 1.27
Kidney	6.77 ± 1.86	2.24 ± 0.44	0.73 ± 0.21	0.29 ± 0.06	0.21 ± 0.07
Heart	6.14 ± 1.07	1.61 ± 0.17	0.41 ± 0.10	0.21 ± 0.05	0.14 ± 0.01
Lung	6.56 ± 1.96	2.10 ± 0.29	0.45 ± 0.14	0.22 ± 0.05	0.14 ± 0.04
Spleen	2.03 ± 0.34	1.04 ± 0.10	0.27 ± 0.05	0.16 ± 0.01	0.12 ± 0.05
Stomach	3.91 ± 0.82	5.99 ± 2.42	5.32 ± 0.92	2.48 ± 0.54	0.98 ± 0.23
Small intestine	5.93 ± 0.87	21.1 ± 5.28	44.3 ± 6.65	56.5 ± 17.5	27.1 ± 15.4
Large intestine	2.14 ± 0.21	2.13 ± 0.15	1.92 ± 0.24	9.48 ± 12.3	50.4 ± 14.0
Bladder	1.46 ± 0.53	1.52 ± 0.71	2.17 ± 2.24	2.15 ± 1.76	1.34 ± 0.81
Bone	1.18 ± 0.10	0.73 ± 0.10	0.40 ± 0.04	0.66 ± 0.16	1.08 ± 0.06
Muscle	2.40 ± 0.60	1.10 ± 0.13	0.33 ± 0.12	0.23 ± 0.06	5.90 ± 0.09

SUPPLEMENTARY MATERIALS AND METHODS

Reagents and instruments

THK-5351 and its tosylated precursor for THK-5351 (THK-5352) were custom-synthesized by Tanabe R&D Service Co. (Osaka, Japan) and prepared as previously described. The other THK compounds were previously described (*32*). All reagents were commercially available unless otherwise stated. Flash chromatography was carried out using Hi-Flash™ or Universal™ columns (Yamazen science, Inc., Osaka, Japan). ^{1}H-NMR spectra were recorded on a Bruker AVANCE600 (Bruker, Billerica) or JEOL JNM-ECA600 (600 MHz). Mass spectra were obtained on a MALDI LTQ XL (Thermo Scientific, Waltham). For MALDI-IT-MS, 2,5-dihydroxybenzonic acid was used as a matrix. Chemical shifts (δ) are given from TMS (0 ppm), and coupling constants are expressed in hertz (Hz). Multiplicity was defined with the following abbreviations: s = singlet, d = doublet, t = triplet, dd = double doublet, m = multiplet, br = broad.

1-fluoro-3-((2-(pyridin-3-yl)quinoline-6-yl)oxy)propan-2-ol (SMBT-0)(1)

Sodium carbonate (185 mg, 2.37 mmol), bis(triphenylphosphine)palladium(II) chloride (7.4 mg, 0.01 mmol) and water (0.75 mL) were added to a solution of 6-(2-((tert-buthyldimethysilyl)oxy)-3-fluoropropoxy)-2-chloroquinoline (320 mg, 0.87 mmol) and 3-(4,4,5,5-tetramethyl-1,3,2-dioxaneborolan-2-yl)pyridine (212 mg, 1.03 mmol) in 1,2-dimethoxyethane (1.7 mL). The mixture was refluxed for 1 h at

90 °C. The reaction was cooled and quenched with water and extracted with ethyl acetate. The combined organic layers were washed with water, dried over with anhydrous magnesium sulfate, filtered, and evaporated and the residue was obtained. The residue was purified by flash chromatography (gradient hexane/ethyl acetate from 74/26 to 53/47) to yield 261.16 mg. A mixture of the crude product (150 mg) and tetrabutylammonium fluoride solution (730 µL, 0.73 mmol) in tetrahydrofuran (2 mL) was stirred at room temperature for 2 h. The reaction mixture was quenched with water and extracted with ethyl acetate. The combined organic layers were washed with brine, dried over with anhydrous magnesium sulfate, filtered, and evaporated. The residue was purified by flash chromatography (gradient hexane/ethyl acetate from 67/33 to 46/54, and then ethyl acetate/methanol 80/20) to yield 81 mg of **3** as a white solid (75%, 2 steps). ^{1}H NMR (600 MHz, DMSO-d_6) δ 4.10-4.20 (3H, m), 4.49-4.63 (2H, m), 5.56 (1H, d, J = 4.8 Hz), 7.46-7.48 (2H, m), 7.57 (1H, dd, *J* = 4.8, 8.4 Hz), 8.02 (1H, d, *J* = 10.2 Hz), 8.18 (2H, d, *J* = 9.0 Hz), 8.40 (1H, d, *J* = 8.4 Hz), 8.58 (1H, dt, *J* =1.8, 7.8 Hz), 8.67 (1H, dd, *J* = 2.4, 4.5 Hz), 9.41 (1H, d, *J* =1.8 Hz). EI-MS m/z = 298$[M]^+$

(S)-1-((2-chloroquinolin-6-yl)-3-fluoropropan-2-ol (2)

We dropwise added 2.2 M diethyl azodicarboxylate in toluene (1.5 mL, 3.34 mmol) to a solution of 2-Chloro-6-hydroxyquinoline (500 mg, 2.78 mmol), (*R*)-(+)Glycidol (184 µL, 2.78 mmol), and

triphenylphosphine (860 mg, 3.34 mmol) in CH_2Cl_2 (3 mL) at 0 °C. The mixture was stirred at 0 °C for 1 h and at 30 °C for 24 h. The solvent was removed *in vacuo*, and the residue was purified by silica gel chromatography (gradient hexane/ethyl acetate from 64/16 to 53/37) to give crude product (458 mg) as a white solid. A mixture of the crude product (436 mg), KHF_2 (216 mg, 2.77 mmol), tetra-*n*-butylammonium dihydrogen trifluoride (558 mg, 1.85 mmol), and chlorobenzene (1 mL) was stirred at 120 °C for 7 h. The reaction mixture was quenched with K_2CO_3 solution in an ice bath and extracted with ethyl acetate. The combined organic layers were washed with water, dried over with anhydrous magnesium sulfate, filtered, and evaporated. The residue was purified by flash chromatography (gradient hexane/ethyl acetate from 73/27 to 52/48) to yield 203 mg of **1** as a white solid (43%, 2 steps). MALDI-IT-MS m/z 256$[M+H]^+$

(S)-1-fluoro-3-((2-(6-methlpyridin-3-yl)quinoline-6-yl)oxy)propan-2-ol (SMBT-1) (3)

Sodium carbonate (251 mg, 2.37 mmol), bis(triphenylphosphine)palladium(II) chloride (5.6 mg, 0.008 mmol) and water (0.75 mL) were added to a solution of 1 (202 mg, 0.79 mmol) and 2-methyl-5-(4,4,5,5-tetramethyl-1,3,2-dioxaneborolan-2-yl)pyridine (208 mg, 0.95 mmol) in 1,2-dimethoxyethane (1.7 mL). The mixture was refluxed for 5 h at 90 °C. The reaction was cooled, quenched with water, and extracted with ethyl acetate. The combined organic layers were washed with water, dried over with anhydrous magnesium sulfate, filtered, and evaporated. The residue was purified by flash chromatography (gradient

hexane/ethyl acetate from 10/90 to 0/100) to yield 112 mg (0.36 mmol) of **2** (SMBT-1) as a white solid (46%). ^{1}H-NMR (600 MHz, $CDCl_3$) δ 9.18 (s, 1H), 8.41-8.34 (m, 1H), 8.11 (d, *J* = 8.9 Hz, 1H), 8.06 (d, *J* = 8.9 Hz, 1H), 7.82 (d, *J* = 8.2 Hz, 1H), 7.42-7.36 (m, 1H), 7.30 (d, *J* = 7.5 Hz, 1H), 7.17-7.10 (m, 1H), 4.74-4.65 (m, 1H), 4.65-4.56 (m, 1H), 4.40-4.29 (m, 1H), 4.27-4.19 (m, 2H), 2.64 (s, 3H). MALDI-IT-MS m/z = 313 $[M+H]^+$

(S)-1-fluoro-3-((2-(2-methlpyridin-3-yl)quinoline-6-yl)oxy)propan-2-ol (4)

The compound was prepared using the same procedure as 2 starting from **1** and 2-methyl-3-((4,4,5,5-tetramethyl-1,3,2-dioxabrolan-2-yl)pyridine, yielding 3 as a white solid 37 mg, 21%). ^{1}H-NMR (600 MHz, DMSO-d_6) δ 8.54 (m, 1H), 8.37 (d, *J* = 8.5 Hz, 1H), 7.97 (d, *J* = 9.0 Hz, 1H), 7.90-7.89 (m, 1H), 7.72 (d, *J* = 8.5 Hz, 1H), 7.49-7.46 (m, 2H), 7.39-7.37 (m, 1H), 5.5 (d, *J* = 4.9 Hz, 1H), 4.62-4.57 (m, 1H), 4.54-4.49 (m, 1H), 4.18-4.11 (m, 3H), 2.57 (s, 3H). MALDI-IT-MS m/z = 313 $[M+H]^+$

(S)-1-fluoro-3-((2-(4-methlpyridin-3-yl)quinoline-6-yl)oxy)propan-2-ol (5)

The compound was prepared using the same procedure as 2 starting from **1** and (4-methylpyridin-3-yl)boronic acid. This yielded **4** as a white solid 14 mg, 7%). ^{1}H-NMR (600 MHz, DMSO-d_6) δ 8.65 (s, 1H), 8.50 (d, *J* = 5.0 Hz, 1H), 8.38 (d, *J* = 8.5 Hz, 1H), 7.97 (d, *J* = 9.1 Hz, 1H), 7.73 (d, *J* = 8.5 Hz, 1H), 7.49-

7.46 (m, 2H), 7.39 (d, J = 5.0 Hz, 1H), 5.5 (d, J = 4.9 Hz, 1H), 4.62-4.56 (m, 1H), 4.54-4.49 (m, 1H), 4.17-4.12 (m, 3H), 2.43 (s, 3H). MALDI-IT-MS m/z = 313 $[M+H]^+$

(S)-1-fluoro-3-((2-(5-methlpyridin-3-yl)quinoline-6-yl)oxy)propan-2-ol (6)

The compound was prepared using the same procedure as 2, starting from **1** and 4-methyl-3-((4,4,5,5-tetramethyl-1,3,2-dioxabrolan-2-yl)pyridine. This yielded **5** as a white solid 8 mg, 4%). ^{1}H-NMR (600 MHz, DMSO-d_6) δ 8.65 (s, 1H), 8.50 (d, J = 5.0 Hz, 1H), 8.38 (d, J = 8.5 Hz, 1H), 7.97 (d, J = 9.1 Hz, 1H), 7.73 (d, J = 8.5 Hz, 1H), 7.49-7.46 (m, 2H), 7.39 (d, J = 5.0 Hz, 1H), 5.5 (d, J = 4.9 Hz, 1H), 4.62-4.56 (m, 1H), 4.54-4.49 (m, 1H), 4.17-4.12 (m, 3H), 2.43 (s, 3H). MALDI-IT-MS m/z = 313 $[M+H]^+$

(S)-1-fluoro-3-((2-(2-methlpyridin-4yl)quinoline-6-yl)oxy)propan-2-ol (7)

The compound was prepared using the same procedure as 2, starting from **1** and 2-methyl-4-((4,4,5,5-tetramethyl-1,3,2-dioxabrolan-2-yl) pyridine. This yielded **6** as a white solid 29 mg, 30%). ^{1}H-NMR (600 MHz, $CDCl_3$) δ 8.65 (d, J = 5.2 Hz, 1H), 8.17 (d, J = 8.5 Hz, 1H), 8.11 (d, J = 9.2 Hz, 1H), 7.93 (s, 1H), 7.87 (d, J = 8.5 Hz, 1H), 7.81-7.79 (m, 1H), 7.45-7.43 (m, 1H), 7.16 (d, J = 2.7, 1H), 4.73-4.68 (m, 1H), 4.65-4.60 (m, 1H), 4.38-4.33 (m, 1H), 4.25-4.24 (m, 2H), 2.69 (s, 3H). MALDI-IT-MS m/z = 313 $[M+H]^+$

Synthesis of SMBT-1 precursor (THK-5475)

2-(6-methylpyridin-3-yl)quinolin-6-ol (8)

Potassium carbonate (3.4 g, 24.8 mmol), bis(triphenylphosphine)palladium(II) chloride (960 mg, 0.83 mmol), and water (1.44 mL) were added to a solution of 2-Chloro-quinolin-6-ol (1.5 g, 8.3 mmol) and 2-methyl-5-(4,4,5,5-tetramethyl-1,3,2-dioxaneborolan-2-yl)pyridine (2.0 g, 9.1 mmol) in 1,2-dimethoxyethane (70 mL). The mixture was heated for 15 h at 90 °C. The reaction mixture was filtered with celite and eluted with ethyl acetate. The eluent was washed with water and extracted with ethyl acetate. The combined organic layers were washed with water, dried over with anhydrous magnesium sulfate, filtered, and evaporated. The residue was purified by flash chromatography (gradient hexane/ethyl acetate from 30/70 to 0/100) to yield 1.2 g (5.0 mmol) of **7** as a pale yellow solid (61%). EI MS m/z = 236 $[M]^+$

(S)-2-((tert-butyldimethylsilyl)oxy)-3-((2-(6-methylpyridin-3-yl)quinoline-6-yl)oxy)propyl-4-methylbenzensulfonate (9)

We added 2.2 M diethyl azodicarboxylate in toluene (0.13 mL, 0.29 mmol) dropwise to a solution of 3 (57 mg, 0.24 mmol), (*S*)-2-((tert-butyldimethylsilyl)oxy)-3-hydroxypropyl 4-methylbenzenesulfonate (86.5 mg, 0.24 mmol), and triphenylphosphine (76 mg, 0.29 mmol) in CH_2Cl_2 (3 mL) at 0 °C. The mixture was stirred at 0 °C for 1 h and at 30 °C for 24 h. The solvent was removed *in vacuo*, and the residue was purified by

silica gel chromatography (gradient ethyl acetate/methanol from 100/0 to 93/7) to yield 109 mg (0.18 mmol) of **8** as a white solid (78%). MALDI-IT-MS m/z = 579$[M+H]^+$.

(2S)-3-((2-(6-methylpyridin-3-yl)quinolin-6-yl)oxy)-2-((tetrahydro-2H-pyran-2-yl)oxy)propyl 4-methylbenzenesulfonate (precursor for SMBT-1) (10)

Trifluoroacetate (1 mL) and water (0.25 mL) were added dropwise to **4** (109 mg, 0.24 mmol) in dichloromethane (1.5 mL) at 0 °C. The mixture was stirred at room temperature for 24 h. The reaction mixture was quenched with iced water and potassium carbonate solution to adjust the mixture to pH 8 and extracted with ethyl acetate. The combined organic layers were washed with water, dried over with anhydrous magnesium sulfate, filtered, and evaporated. The residue was purified by flash chromatography (gradient hexane/ethyl acetate from 10/90 to 0/100) to yield 58 mg of a white solid containing the product. A mixture of the present product (58 mg), 3,4-dihydro-2H-pyran (233 µL, 2.5 mmol), para-toluenesulfonic acid monohydrate (43 mg, 0.25 mmol), and chloroform (3 mL) was stirred at room temperature for 10 min. After adjusting to pH 8 using triethyl amine, the reaction mixture was evaporated. The residue was purified by flash chromatography (gradient hexane/ethyl acetate from 11/89 to 0/100) to yield 23 mg of **9** as a white solid (21%, 2 steps). ^{1}H-NMR (597 MHz, $CDCl_3$) δ 9.18 (d, J = 13.7 Hz, 1H), 8.39 (t, J = 8.5 Hz, 1H), 8.10 (d, J = 8.2 Hz, 1H), 8.00-8.04 (m, 1H), 7.85-7.64 (m, 4H), 7.58-7.50 (m, 1H), 7.49-7.44 (m, 2H), 7.33-7.27

(m, 3H), 5.51-5.17 (m, 1H), 4.42-4.17 (m, 2H), 4.17-4.05 (m, 4H), 2.64 (d, J = 6.8 Hz, 3H), 2.38 (s, 2H), 2.04 (s, 3H), 1.26 (t, J = 7.2 Hz, 6H), 0.88 (t, J = 6.8 Hz, 1H). MALDI-IT-MS m/z = 549$[M+H]^+$.

Supplemental Scheme 1. Synthesis of 1

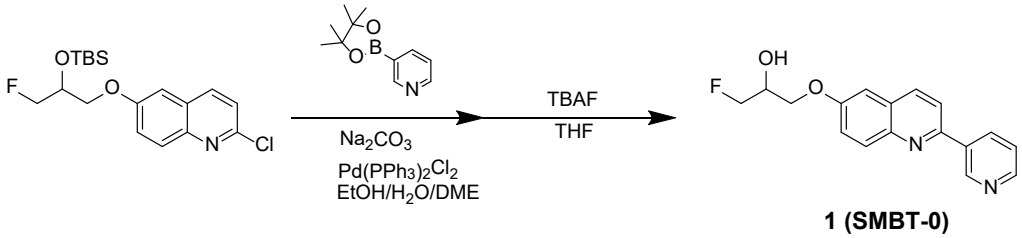

1 (SMBT-0)

Supplemental Scheme 2. Syntheses of 3 (SMBT-1), 4, 5, and 6

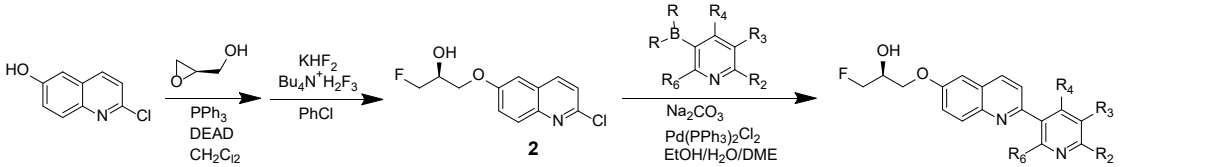

= CH = H (SMBT-1)
3: R_2 $_3$, R_3, R_4, R_6
4: R_2, R_3, R_4 = H, R^6 = CH^3 (SMBT-2)
5: R_2, R_3, R_6 = H, R^4 = CH^3 (SMBT-3)
6: R_2, R_4, R_6 $_3$ $_3$ (SMBT-4)

Supplemental Scheme 3. Synthesis of 7

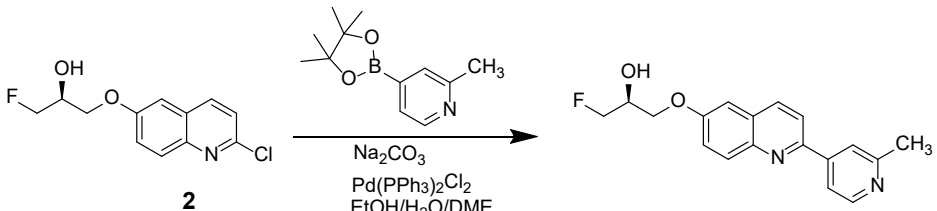

2

7 (SMBT-5)

Supplemental Scheme 4. Synthesis of SMBT-1 precursor (THK-5475)

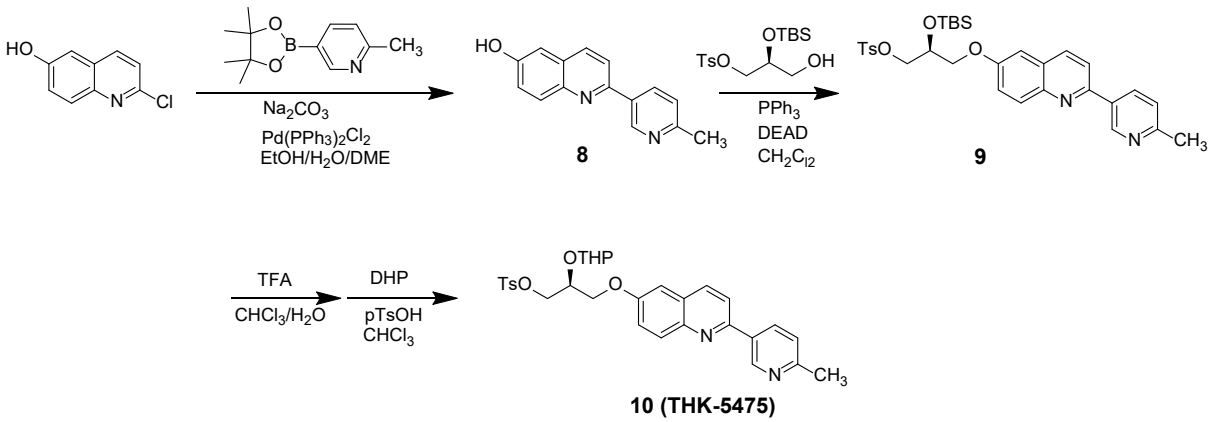

Supplemental Data

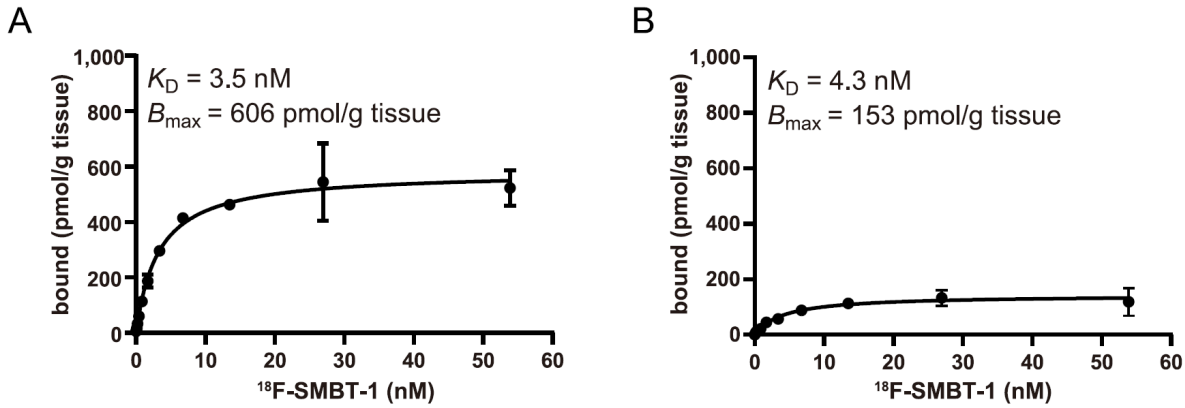

Supplementary Figure 1: *In vitro* saturation binding of ^{18}F-SMBT-1 against (A) human brain homogenates (Alzheimer's disease, 81-year-old male) and (B) mouse brain homogenates (C57BL/6, 12-month male).

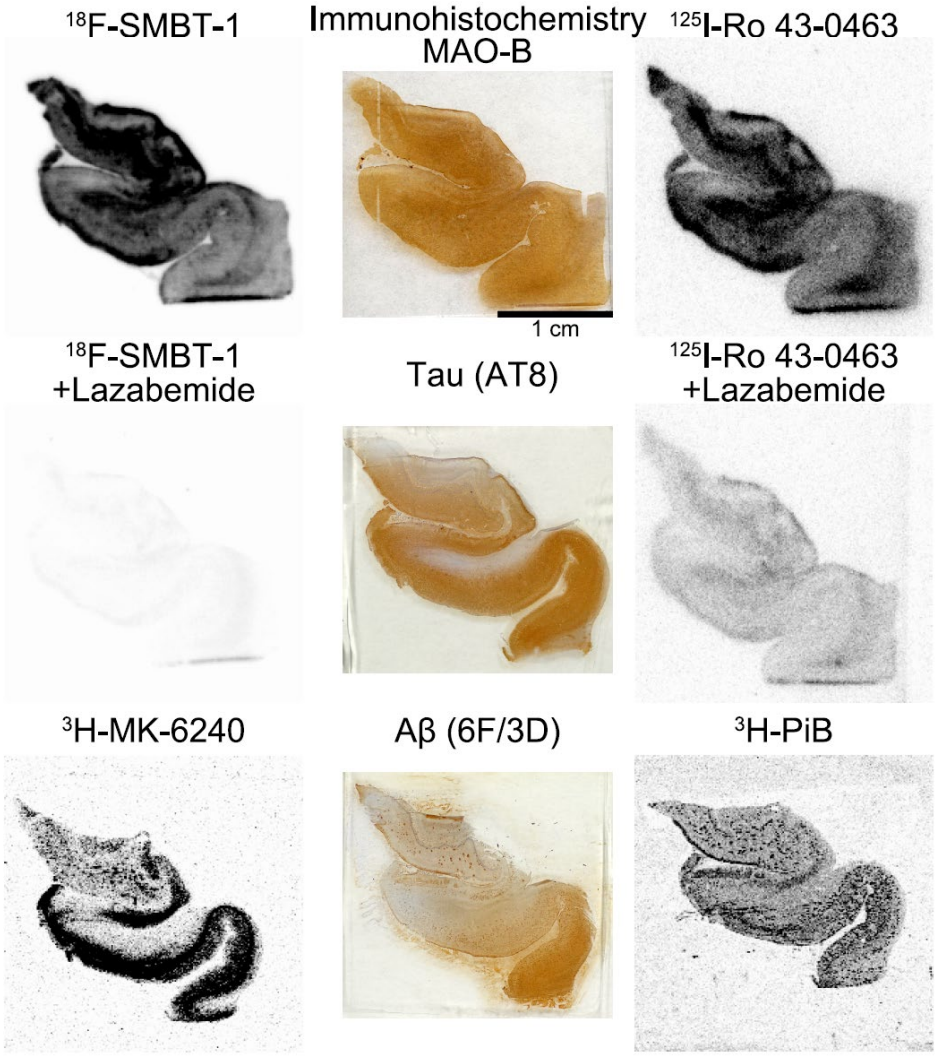

Supplementary Figure 2: Comparative *in vitro* autoradiography of ^{18}F-SMBT-1, ^{125}I-Ro 43-0463, ^{3}H-MK-6240, and ^{3}H-PiB in the hippocampal section of a patient with Alzheimer's disease (81-year male). Adjusted sections were stained by anti- monoamine oxidase-B (MAO-B), anti-pTau (AT8), and anti-amyloid-β (6F/3D) antibodies.

Supplementary Table 1 Summary of the procedure and conditions for radiosynthesis of ^{18}F-SMBT-1.

Steps	Operations	Conditions
1	$^{18}F^-$ elution from QMA-C	Krypt222 (8 mg), K_2CO_3 (1.5 mg), MeCN (0.45 mL), H_2O (0.13 mL)
2	Azeotropic drying	CH_3CN (1 mL), 110°C
3	Addition of precursor	2.0 mg in DMSO (0.45 mL)
4	Fluorination	110 °C, 10 min
5	Deprotection	aq. HCl (2.0 M, 0.2 mL), 110 °C, 3 min
6	Reaction quench	0.2 M AcOK (4 mL)
7	Extraction of the product	Sep-PaktC18 Light, Washing (H_2O, 4 mL), Elution (70% EtOH, 0.7 mL)
8	Dilution of the eluate	With H_2O (1.2 mL)
9	HPLC separation	Column: Inertsil ODS-4 (10 mm × 250 mm, particle size: 5 μm), Mobile phase: MeCN/20 mM NaH2PO4 (33/67), Flow rate: 5.0 mL/min, UV wavelength = 340 nm, Collection: Radioactive peak @ 20～21 min
10	Extraction of the product	(1) Fraction + H_2O(25 mL) + Ascorbic acid injection (25%, 1mL) (2) Sep-Pak-tC18 → Washing (H_2O, 10 mL) → Elution (EtOH, 4 mL)
11	Formulation	(1) Eluate + Ascorbic acid injection* (25%, 0.2mL) + Polysorbate 80 (5% EtOH, 0.8 mL) (2) Rotary evaporation (70°C, 4-5 min) → Saline (10 mL) (3) Sterilization: Millex-GV Syringe Filter

Supplementary Table 2 Binding affinity of compounds against recombinant monoamine oxidase-B (MAO-B)

Compound	Chemical structure	MAO-B (IC_{50}, nM)
THK-5351	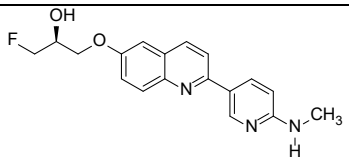	5.2
THK-5105	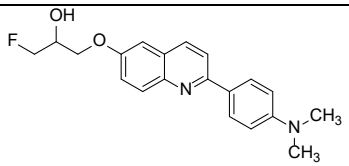	5.8
THK-5378	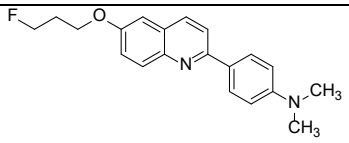	426.7
THK-5451	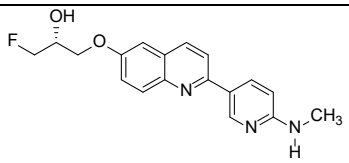	20.4
SMBT-0	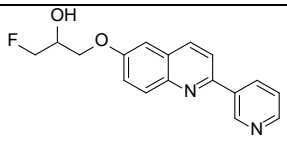	60.6
SMBT-1	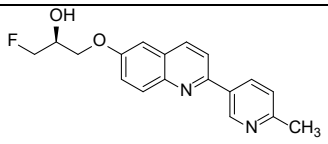	4.2
SMBT-2	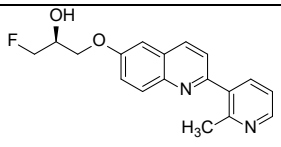	555.0

SMBT-3	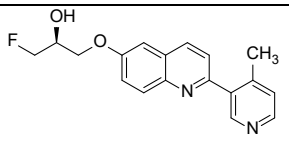	294.0
SMBT-4	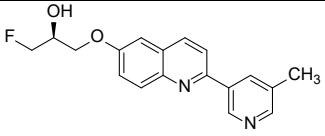	12.2
SMBT-5	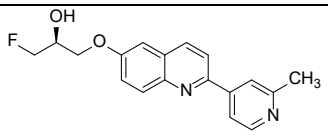	12.9
Rasagiline	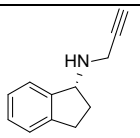	3.1
Lazabemide	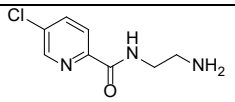	1.9
Safinamide	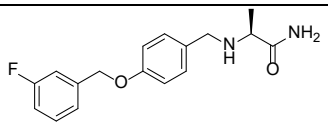	1.4

Supplementary Table 3: Inhibitory effects of SMBT-1 on radioligand binding to amyloid-β, tau, MAO-A, and MAO-B

Assay system	IC_{50} (nM)	
	SMBT-1	Positive substance
Amyloid-β (AD brain homogenate)	1,000	2.2 (PiB)
Tau (AD brain homogenate)	1,000	1.2 (MK-6240)
MAO-A (recombinant)	713	2.6 (Fluoroethyl harmine)
MAO-B (recombinant)	4.2	3.1 (Rasagiline)

Supplementary Table 4: Inhibitory effects of SMBT-1 on radioligand binding to various receptors, ion channels, and transporters

Assay system	Inhibition (%)	
	SMBT-1	Positive substance
Adenosine A1 (Human)	11.72	99.73 (DPCPX)
Adenosine A2a (Human)	11.95	100.00 (CGS21680)
α1A-Adrenergic	2.23	100.00 (Prazosin)
α1B-Adrenergic	0.26	100.00 (Prazosin)
α2A-Adrenergic (Human)	14.97	99.60 (Rauwolscine)
α2B-Adrenergic (Human)	1.98	100.00 (Rauwolscine)
β1-Adrenergic (Human)	0.00	100.00 ((±)-Propranolol)
β2-Adrenergic (Human)	1.63	100.00 ((±)-Propranolol)
Androgen	14.85	100.00 (Testosterone)
Angiotensin AT1 (Human)	0.00	100.00 (Angiotensin II)
Bradykinin B1 (Human)	0.00	100.00 (Lys-(des-Arg^9, Leu^8)-Bradykinin)
Bradykinin B2 (Human)	3.30	97.85 (HOE140)
Ca channel (Type L, Benzothiazepine)	2.79	100.00 ((+)-*cis*-Diltiazem)
Ca channel (Type L, Dihydropyridine)	2.94	100.00 (Nitrendipine)
Ca channel (Type N)	0.00	100.00 (ω-Conotoxin GVIA)
Dopamine D1 (Human)	3.38	98.72 (R(+)-SCH-23390)
Dopamine D2 short (Human)	8.18	99.64 ((+)-Butaclamol)
Dopamine D3 (Human)	3.34	99.79 ((±)-7-OH-DPAT)
Dopamine D4.2 (Human)	2.86	100.00 (Haloperidol)
Dopamine transporter (Human)	37.94	100.00 (GBR12909)
Estrogen	2.02	98.83 (β-Estradiol)
Endothelin ETA (Human)	0.00	99.75 (Endothelin-1 human)
Endothelin ETB (Human)	0.00	100.00 (Endothelin-1 human)
GABA A (Agonist site)	2.05	97.50 (Muscimol)
GABA A (BZ central)	0.02	99.96 (Diazepam)
GABA B	5.95	99.94 (GABA)

GABA transporter	2.31	96.22 (GABA)
Glucocorticoid (Human)	4.58	100.00 (Dexamethasone)
Glutamate (Kainate)	0.00	99.72 (Kainic acid)
Glutamate (NMDA agonist site)	0.00	99.77 (L-Glutamic acid)
Glutamate (NMDA glycine site)	4.39	99.78 (MDL105,519)
Glutamate (NMDA phencyclidine site)	0.20	99.92 ((+)-MK-801)
Histamine H1 (Human)	12.18	100.00 (Pyrilamine)
Histamine H2 (Human)	0.00	98.88 (Cimetidine)
Histamine H3 (Human)	2.09	99.88 ((R)(−)-α-Methyl histamine)
Imidazoline (Central)	6.15	100.00 (Guanabenz)
K channel KATP	9.42	100.00 (Glybenclamide)
K channel SKCa	0.50	99.92 (Apamin)
Leukotriene B4	2.92	100.00 (Leukotriene B_4)
Leukotriene D4	0.00	100.00 (Leukotriene D_4)
Muscarinic M1 (Human)	6.12	99.74 (Atropine)
Muscarinic M2 (Human)	0.84	99.84 (Atropine)
Muscarinic M3 (Human)	0.00	99.98 (Atropine)
Na channel Site 2	6.84	100.00 (Dibucaine)
Neurokinin NK1 (Human)	1.71	95.54 (L-703,606)
Neuropeptide Y1 (Human)	0.00	99.33 (Neuropeptide Y human)
Neuropeptide Y2 (Human)	5.15	100.00 (Neuropeptide Y human)
Norepinephrine transporter (Human)	15.94	99.36 (Desipramine)
Nicotinic (Human)	0.30	97.79 ((±)-Epibatidine)
Opiate δ (Human)	15.10	99.51 (Naltriben)
Opiate κ (Human)	6.11	99.41 (U-69593)
Opiate μ (Human)	4.72	98.45 (DAMGO)
PAF	5.14	99.80 (PAF)
Serotonin 5HT1A (Human)	0.96	100.00 (Serotonin)
Serotonin 5HT2A (Human)	2.49	99.90 (Ketanserin)
Serotonin 5HT3 (Human)	6.65	99.43 (Tropisetron)
Serotonin transporter (Human)	15.07	99.68 (Imipramine)

Sigma σ1	4.70	100.00 ((+)-Pentazocine)
Sigma σ2	0.49	99.99 (Haloperidol)
Vasopressin V1	10.86	99.53 ([Arg^8]-Vasopressin)

Supplementary Table 5: Average absorbed dose estimates [µGy/MBq] for the target organs

Target Organs	SMBT-1 (male)	SMBT-1 (Female)
Adrenal	12.2	15.2
Brain	4.13	5.27
Breasts	9.54	11.2
Gallbladder wall	16.7	21.2
Lower large intestine wall	34.5	45.9
Small intestine	80.8	114.0
Stomach wall	15.6	19.5
Upper large intestine wall	42.2	57.9
Heart wall	6.46	8.28
Kidneys	8.79	11.4
Liver	11.3	16.7
Lungs	6.09	7.81
Muscle	7.6	9.72
Ovary	-	28.4
Pancreas	13.7	16.7
Red marrow	12.4	14.8
Osteogenic cells	17.9	21.8
Skin	8.57	10.2
Spleen	6.87	8.9
Testis	11.0	-
Thymus	10.3	12.9
Thyroid	10.7	12.1
Urinary bladder wall	14.7	15.8
Uterus	-	25.7
Total body	12.2	15.6
Effective dose [µSv/MBq]	**12.2**	**21.3**